HUNGARIAN JOURNAL OF
INDUSTRY AND CHEMISTRY
Vol. 52(2) pp. 1–9 (2024)
hjic.mk.uni-pannon.hu
DOI: 10.33927/hjic-2024-13

EFFICIENCY IMPROVEMENTS OF SOLAR COLLECTORS BY TURBULENCE PROMOTERS

ABDELKADER LAHCENE[1], NABIL BENAMARA[1], MOHAMED BENGUEDIAB[1*] AND ABDELILAH BENAZZA[1]

1 Laboratory of Materials and Reactive Systems, Department of Mechanical Engineering, Faculty of Technology, Universite Djillali Liabes de Sidi Bel Abbes, Sidi Bel Abbes, 22000, ALGERIA

Due to their sustainability and availability, solar thermal collectors are frequently employed to heat homes. This technique has the advantage of being non-polluting and efficient. The poor thermal efficiency of classic solar air heaters is caused by the low convective heat transfer coefficient between the absorber plate and the circulating fluid. The aim of this research is to determine the optimal configuration of flow disruptors - including their shape, size and distribution - in order to streamline the efficiency of the solar collector while maintaining affordable costs.

Keywords: efficiency, solar collectors, improved turbulence promoters, optimization

1. Introduction

Studies have highlighted the importance of solar thermal collectors for heating homes due to their efficiency and non-polluting nature. The efficiency of solar receivers for thermal applications, like home heating, relies on optimizing the solar angle of incidence as well as convective heat transfer coefficients between the absorber plate and heat transfer fluid [1]-[2]. Creating a laminated sublayer on the lower side of the absorber plate can help increase convective heat transfer coefficients and improve the overall performance of solar air heaters [3]-[4].

To tackle this problem, previous research has suggested installing turbulence promoters on the bottom of the absorber plate. This approach aims to disrupt the formation of the viscous sublayer to enhance the thermal efficiency of solar collectors [5]-[9]. Previous studies [10]-[12] extensively investigated the effectiveness and feasibility of harnessing solar energy. These studies examined various techniques and advancements to optimize the utilization of this renewable energy source. Their findings have significantly contributed to the enhancement of solar technologies as well as led to a deeper comprehension of their performance and practical application. In conclusion, solar thermal collectors are an efficient and environmentally-friendly solution for heating homes. By incorporating turbulence promoters into the absorber plate, the thermal efficiency of solar collectors can be improved as they disrupt the viscous sublayer.

Previous research has played a significant role in the optimization of solar energy utilization, making valuable contributions to its advancement and broader acceptance.

A study on improving thermal efficiency in Hungary examined home heating using only solar power, including the heat output, storage capacity and cycle timing. It offers ideas for district heating and power generation as well as a workable strategy for heat storage [13].

Another study introduced a new sensible heat storage system designed for solar energy using a spiral flow-path layout to improve efficiency. Results show superior levels of efficiency compared to traditional systems [14].

A study proposed the use of inclined baffles at the top of a flat solar collector [15]. A heat transfer analysis was conducted using the RNG k-ε model and Fluent software. The results showed that the best level of heat transmission occurs when the baffles are placed at the bottom of the collector. This configuration makes it possible to optimize the efficiency of the flat-plate solar air collector.

Using COMSOL Multiphysics 5.4, a performance simulation of a flat-plate solar air collector with rectangular baffles was performed [16]. The intent of this sensor was to heat both air and water. This approach makes it possible to exploit solar energy for different thermal needs.

An experimental study conducted by Chabane [17] in Biskra, Algeria focused on the reduction of direct heat losses from a solar air collector. The experimental model included double glazing and enlarged the space between

Received: 3 Apr 2024; Revised: 22 Apr 2024;
Accepted: 24 Apr 2024
*Correspondence: benguediabm@gmail.com

Table 1: Thermophysical properties

Properties	Al absorber plate	Fluid/Air
ρ (kg/ m^3)	2719	1.225
λ (W/m k)	202.4	0.0242
Cp (J/kg k)	871	1006.43
μ (N.s/ m^2)		1.7894e-05

the double glazing to reduce such losses. Experimental results indicated that a reduction in the forward thermal loss of the solar air collector is achieved with the integration of additional glazing.

These investigations highlight different approaches to improve the efficiency and reduce the thermal losses of flat-plate solar air collectors. In order to make better use of solar energy in air and water heating, the use of baffles and double glazing are techniques that are often used.

In a study conducted by Amraoui [18], the solar collector was modeled using computational fluid dynamics (CFD) software to better understand its heat transfer capabilities. Ansys Workbench was used to model the air intake and manifold in three dimensions, while Ansys ICEM was used to generate the grille.

Abdi [19] used the finite volume method to investigate the flat-plate solar air collector and used the Ansys Fluent CFD simulation to solve the system of equations in the computational and thermal analysis of the collector.

Kumar et al. [20] explored the addition of cylindrical baffles perpendicular to the dynamic airflow between the absorber and the insulation of the flat-plate solar air collector. This configuration aims to increase the convective heat transfer coefficient between the air and absorber, thereby improving the efficiency of the sensor.

To enhance the efficiency of flat-plate solar air collectors, an original concept of artificial roughness was introduced to optimize heat transfer by incorporating roughness into the surface of the absorber [21].

In a separate study, trials were conducted to quantify the rate of heat transfer in an airflow channel with different baffle shapes, including triangular, wedge and rectangular designs [22]. This study showed that a triangular baffle offers a significant thermal improvement compared to the other baffles studied.

These studies highlight different approaches and techniques such as CFD modeling, the addition of baffles as well as the use of artificial roughness models to enhance the efficiency and heat transfer of flat-plate solar air collectors.

An investigation was conducted on the heat exchange characteristics of a fluid flowing in a rectangular conduit equipped with different shapes of baffles such as rectangular, triangular, circular and trapezoidal. The findings showed that raising the height of the baffle contributes to an increase in the Nusselt number, indicating an improvement in heat exchange [23].

Furthermore, a research investigation was conducted [24] to analyze the thermal-hydraulic properties of a channel fitted with a V-shaped deflector, wherein the angle of inclination varied in relation to the horizon. They found that the highest level of heat exchange is achieved when the baffle is tilted at an angle of 45°.

Another study on heat exchange in turbulent airflow through a container equipped with one or more baffles was conducted [25]. Two baffles were tilted at an angle of 45° in this study, showing that by placing them in opposite positions, the rate of heat exchange increases by up to 6%.

Other studies have also examined the impact of obstacles and baffles on heat transfer. These studies were conducted both numerically and experimentally, analyzing laminar and turbulent flows. Some studies are limited to two-dimensional cases. The objective of these researches is to rationalize the geometric forms of the baffles and understand their effect on heat transfer with regard to the absorber.

These researches seek to improve the design of flat-plate solar air collectors by employing turbulence promoters and barriers to optimize the efficiency of heat transfer and contribute to a better understanding and optimization of these systems for a more efficient use of solar energy.

2. CFD simulation

CFD is employed to examine a two-dimensional solar air heater conduit featuring artificially roughened ribs. The resolution of the conservation equations of mass, momentum and energy is conducted using the finite volume method with the Ansys Fluent 16.0 software. The analysis is based on several hypotheses:

1. The flow is assumed to be stable, two-dimensional and turbulent.
2. The flow through the conduit is considered to be single-phase.
3. The surfaces in contact with the fluid are the walls, which are subjected to a no-slip boundary condition.
4. The fluid within the operating range of the solar heater unit is assumed to be incompressible as variations in density along its width and height are negligible.
5. The air and aluminum absorber plates are assumed to exhibit constant thermophysical properties throughout the analysis (*Table 1*).
6. Minor radiant heat losses and other losses are taken into account in this analysis. These assumptions help simplify the problem and focus on the key aspects of flow and heat transfer within the solar heater unit conduit. The simulation results will provide valuable insights into the performance of the system and enable the optimization of the rib design to enhance heat transfer efficiency.

Table 2: Geometric dimensions and operating conditions

Geometric parameters	Interval
Duct inlet section: L1 (mm)	245
Duct outlet section: L3 (mm)	115
Test section of duct: L2 (mm)	280
Thickness: e (mm)	1.00 - 1.14
Hydraulic Diameter of conduit: D (mm)	33.33
Rib pitch: p (mm)	20 - 10
Ratio p/e	14.28 - 17.14
Ratio e/D	0.042 - 0.030

2.1. Geometric model

A rectangular duct as a calculation domain for the solar heater unit is presented in this study. The dimensions of the duct (*Figure 1*) are its height (H) = 20 mm, width (W) = 100 mm and total length (L) which is divided into three sections: an inlet section ($L1$), a second test section ($L2$) and a third outlet section ($L3$). *Figure 2* shows three different types of rib shape (triangular, square, semi-circular). The influence of the relative roughness height (e/D), relative roughness pitch (p/e) and the Reynolds number (Re) range of 3500 to 18000 on the system is presented. By choosing these parameters, different configurations are explored and a wide range of operating conditions for solar heaters covered in this study. The objective is to assess how the relative roughness height, relative roughness pitch and Reynolds number impact the performance of the system, ultimately optimizing the design of the solar heater unit in order to enhance its heat transfer efficiency.

The absorber plate is heated with a constant heat flux (q) of 1000 W/m^2 in this study. The geometric dimensions and operating conditions are summarized in *Table 2*.

2.2. Mesh generation

The accuracy of the results obtained in the numerical simulation essentially depends on the mesh. In this study, the numerical solutions are obtained using a non-uniform mesh structure generated by applying Ansys 16.0 software. For the analysis, a grid containing 300,665 cells was adopted after careful verification of the values of the Nusselt number and the friction factors.

The non-uniform mesh structure of the solar air heating conduit is illustrated in *Figure 3*. A non-uniform grid enhances the resolution of velocity and temperature gradients through the duct, leading to more accurate results. This approach also reduces the computational time required to obtain a convergent solution. The non-uniform mesh structure used in this study will provide reliable and accurate results for heat exchange in the solar air heating duct.

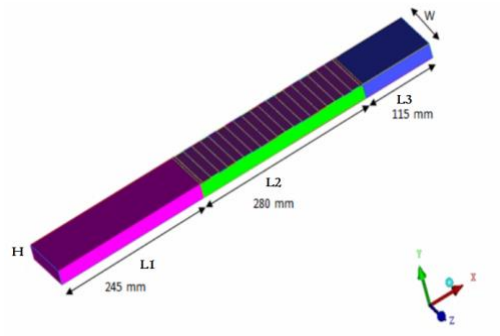

Figure 1: Proposed 3D diagram of SAH

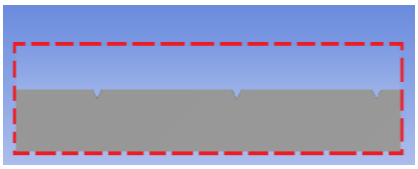

(a)

(b)

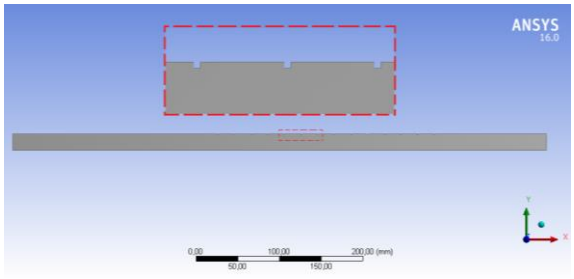

(c)

Figure 2: Proposed SAH with three shapes of ribs: a) triangular, b) square, c) semi-circular

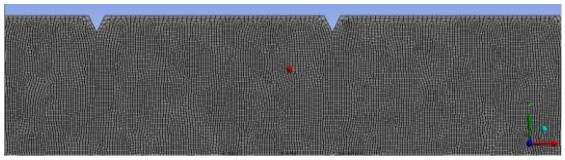

Figure 3: Non-uniform wire mesh of the pipe of the solar air heater

2.3. Mesh sensitivity

The impact of the mesh size on variations in the Nusselt number (Nu) and coefficient of friction (f_r) are illustrated

Table 3: Mesh sensitivity

Number of elements	Elements size	Nu	ΔP (Pa)	f_r	Relative error of Nu (%)	Relative error of f_r (%)
51710	0.50	34.486	1.1989	0.0324	--	--
79997	0.40	36.455	1.0935	0.0296	1.9690	0.0028
103095	0.35	37.457	1.3766	0.0372	1.0018	0.0076
167657	0.27	37.952	1.3487	0.0365	0.4946	0.0007
300665	0.15	37.895	1.4804	0.0401	0.0057	0.0036

in *Table 3* to demonstrate their sensitivity. It was found that when the grid number (element number) was larger, the relative error of the Nusselt number and coefficient of friction was almost zero.

3. Governing equations

The problem of convective heat transfer in a solar collector, which is equipped with an absorber plate that is artificially rough, is solved using the equations that govern continuity, conservation of momentum and energy. These equations are well-established and can be expressed in the two-dimensional Cartesian coordinate system as follows.

The flow in the system is considered to be two-dimensional and stable, moreover, the fluid is incompressible. Additionally, the radiation heat transfer from the conduit into the environment is assumed to be negligible. The continuity equation governing the system is expressed as follows:

$$\frac{\partial u}{\partial x}+\frac{\partial v}{\partial y}=0 \tag{1}$$

The equations governing momentum in the system are provided below:

$$u\frac{\partial u}{\partial x}+v\frac{\partial u}{\partial y}=-\frac{1}{\rho}\frac{\partial p}{\partial x}+v\left(\frac{\partial^2 u}{dx^2}+\frac{\partial^2 u}{\partial y^2}\right) \tag{2}$$

$$u\frac{\partial v}{\partial x}+v\frac{\partial v}{\partial y}=-\frac{1}{\rho}\frac{\partial p}{\partial y}+v\left(\frac{\partial^2 v}{dx^2}+\frac{\partial^2 v}{\partial y^2}\right) \tag{3}$$

The energy equation is given by:

$$u\frac{\partial T}{\partial x}+v\frac{\partial T}{\partial y}=\alpha\left(\frac{\partial^2 T}{\partial x^2}+\frac{\partial^2 T}{\partial y^2}\right) \tag{4}$$

3.1. Performance of the Solar Air Heater (SAH)

By analyzing the thermal and hydraulic parameters, the design of the solar thermal unit can be optimized.

3.1.1. Thermal performance

Using the Hottel-Whillier-Bliss equation described by Duffie and Beckman [3], the thermal performance of the solar heater units by taking into consideration the heat transfer process within the collector can be evaluated:

$$Q_u=A_cF_R[I(\tau\alpha)_e-U_L(T_i-T_a)] \tag{5}$$

This equation can be written as follows:

$$q_u=\frac{Q_u}{A_c}=F_R[I(\tau\alpha)_e-U_L(T_i-T_a)] \tag{6}$$

The valuable heat transfer rate resulting from the circulation of air through the duct of a solar heater unit can be determined the following equation:

$$Q_u=mC_p(T_0-T_i)=hA_c\left(T_{pm}-T_{am}\right) \tag{7}$$

The heat transfer coefficient (h) can be enhanced by implementing various active and passive augmentation techniques that increase its value. This enhancement can be quantified using a non-dimensional form called the Nusselt number:

$$Nu_r=\frac{hD}{k} \tag{8}$$

where

$$D=\frac{4(HxW)}{p} \tag{9}$$

For a slick (smooth wall) conduit of a solar heater unit, the Nusselt number can be determined using the Dittus-Boelter equation [26]:

$$Nu_s=0.023Re^{0.8}Pr^{0.4} \tag{10}$$

3.1.2. Hydraulic performance

The drop in pressure (ΔP) indicates the energy consumption of the fan necessary to propel the air across the conduit and is related to the hydraulic performance of a solar heater unit. For a fully developed turbulent flow in a pipe where Re = 50,000, the drop in pressure can be calculated as:

$$f_r=\frac{(\Delta P/L)D}{2\rho vU^2} \tag{11}$$

For a slick conduit of a solar heater unit, the friction factor can be determined using the Blasius equation [27]:

$$f_s=0.0791Re^{-0.25} \tag{12}$$

3.1.3. Thermal and hydraulic effectiveness

When assessing the efficiency of a solar air heater, it is essential to consider the energy expended to propel air and enhance the amount of heat gained. The concept of a solar air heater must be optimized in such a way as to maximize the transfer of thermal energy to the heat transfer fluid while minimizing the electrical consumption of the fan. To analyze the overall performance of a solar air heater, it is necessary to simultaneously evaluate the thermal and hydraulic characteristics of the collector, facilitating the complete evaluation of its thermal-hydraulic performance. The thermal-hydraulic performance parameter (*THPP*) is an important criterion used to evaluate thermal-hydraulic performance by comparing the heat transfer of an artificially rough pipe to that of a slick pipe when subjected to constant ventilation power stresses. This parameter is defined by Webb and Eckert [28] as follows:

$$THPP=\frac{Nu_r/Nu_s}{(f_r/f_s)^{1/3}} \tag{13}$$

The effectiveness of an enrichment device can be determined by obtaining a value greater than one, allowing different devices to be compared and the most efficient one identified. *THPP*, based on a constant ventilation power, is a commonly utilized metric in the literature to assess the relative efficiency of different rib geometries in terms of enhancing heat transfer when ventilation conditions are stable.

4. Analysis of the results

4.1. Model validation

The Fluent code is utilized to simulate the slick conduit using the RNG k-ε turbulence model where the absorber plate is considered to exhibit no artificial roughness. The findings of the Nusselt numbers and friction coefficients obtained are compared with the outcomes taken from the theoretical correlations given in the literature (see *Figures 4* and *5*).

The numerical results obtained from the Nusselt numbers and the friction coefficients are in good agreement with the Dittus-Boelter and Blasius correlations, respectively, whose minimum errors were less than 0.6% and the maximum ones did not exceed 5% (see *Figures 4* and *5*). Indeed, the turbulence model used is validated for this type of flow.

4.2. Analysis of heat transfer

4.2.1. Effect of the relative roughness step

The influence of the Reynolds number on the mean Nusselt number with a fixed *e/D* ratio of 0.042 and varying *p/e* ratio is depicted in *Figure 6*. The results demonstrate that as the Reynolds number and height ratio rise, the average Nusselt number also increases, which can be attributed to the transition of the flow field from a laminar sublayer to a turbulent flow near the wall. Compared to a slick duct, maximum improvements in the average Nusselt number of approximately 53.4% for the triangular, 45.7% for the semi-circular and 25.0% for the square shapes are recorded for a Reynolds number of 18000 in the case of an artificially rough conduit. The design and enhancement of the heat transfer in a solar heater unit is heavily dependent on the incorporation of differently shaped artificially rough elements.

4.2.2. Influence of the relative roughness height on the flow characteristics

The influence of the Reynolds number on the Nusselt number when the fin pitch-to-height ratio is fixed (*p/e* = 14.28) and the ratios of fin thickness to hydraulic diameter varies is illustrated in *Figure 7*. It is observed that simultaneously increasing the Reynolds number and the relative roughness height leads to an increase in the Nusselt number. This phenomenon arises from the

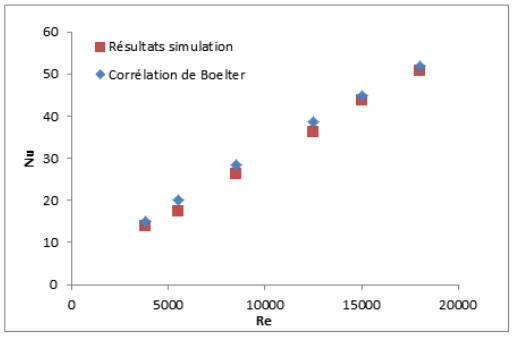

Figure 4: Validation of the Nusselt number calculations

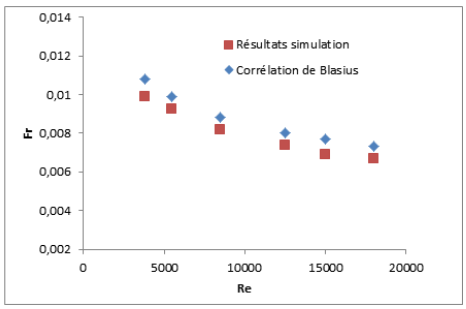

Figure 5: Validation of the friction factor calculations

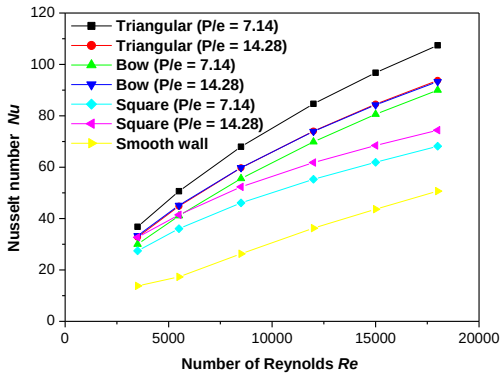

Figure 6: Relationship between the Nusselt number and Reynolds number (*e/D* = 0.042 and *p/e* varies)

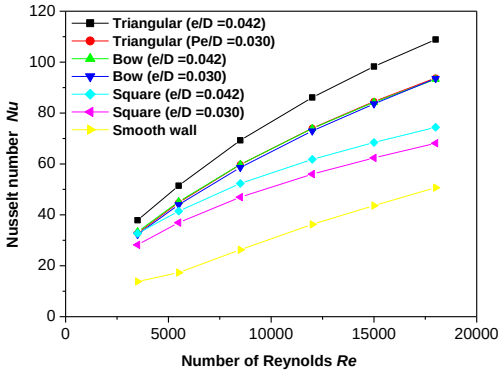

Figure 7: Relationship between the Nusselt number and Reynolds number (*p/e* = 14.28 and *e/D* varies)

generation of turbulence in localized regions, resulting in the mixing of airflows and the formation of vigorous secondary flows. The detachment and reattachment of the free shear layer in the boundary layer, intensified by an increase in the *e/D* ratio, contribute to this flow mechanism. As a result, both local and average heat transfer rates are enhanced. In other words, increasing the Reynolds number and *e/D* ratio causes turbulence, which improves the heat transfer rate.

4.3. Friction factor calculation

4.3.1. Impact of the relative roughness-pitch on the friction factor

The impact of the relative roughness pitch on the friction factor when *e/D* is kept constant at 0.042 is illustrated in *Figure 8*. The findings demonstrate that as the Reynolds number increases, the friction factor decreases. The highest values of the friction factor are obtained when the *p/e* ratio is at its maximum value of 14.28. In this scenario, introducing artificial roughness impacts the primary flow and alters the structure of the turbulent boundary layer, leading to the creation of detachment and reattachment regions in the viscous sublayer as well as an increase in the friction, that is, the flow resistance. In other words, the friction increases by introducing artificial roughness, which can impact the overall efficiency of the enrichment device.

4.3.2. Impact of the relative roughness height on the friction factor

The change in the friction factor with regards to the Reynolds number when the spacing pitch is fixed (*p/e* = 14.28) and *e/D* varies is illustrated in *Figure 9*. The results obtained show that when the Reynolds number increases, the friction factor decreases. When *e/D* is highest at 0.042, the maximum friction factors are obtained due to the increased flow resistance of the rough wall.

4.4. Improvement of the thermal coefficient

Variations in the *THPP* as a function of the Reynolds number at different *e/D* ratios and *p/e* ratios are shown in *Figures 10* and *11*. It was found that in both cases considered, the *THPP* is optimal when the Reynolds number is equal to 5000. At a fixed *e/D* ratio of 0.042, the best *THPP* for improving thermal performance is obtained when the *p/e* ratio for triangular ribs is 7.14 (see *Figure 10*). When the *p/e* ratio is fixed at 14.28, the triangular ribs yield the optimal *THPP* at a maximum *e/D* ratio equal to 0.042 (*Figure 11*).

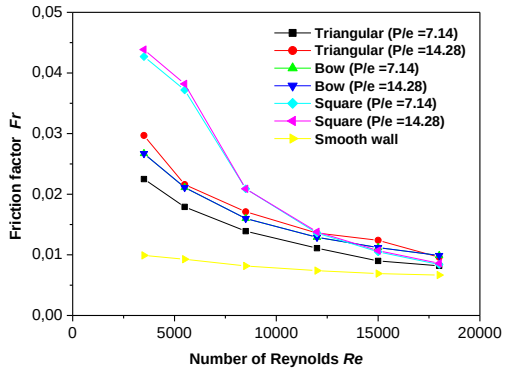

Figure 8: Evolution of the friction factor with regards to the Reynolds number (*e/D* = 0.042 and *p/e* varies)

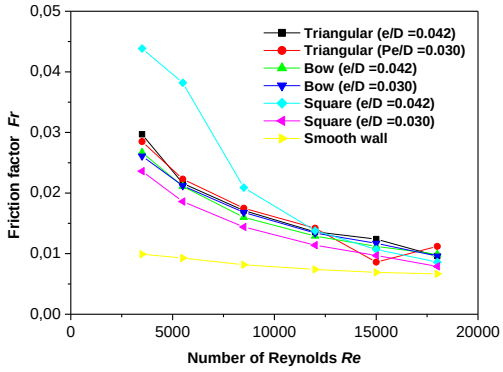

Figure 9: Friction factor vs. Reynolds number (*p/e* = 14.28 and *e/D* varies)

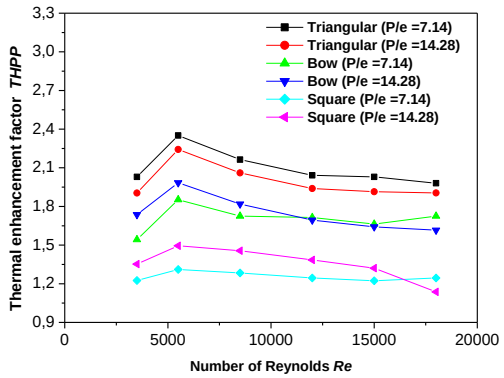

Figure 10: THPP vs. Reynolds number (*e/D* = 0.042 and *p/e* varies)

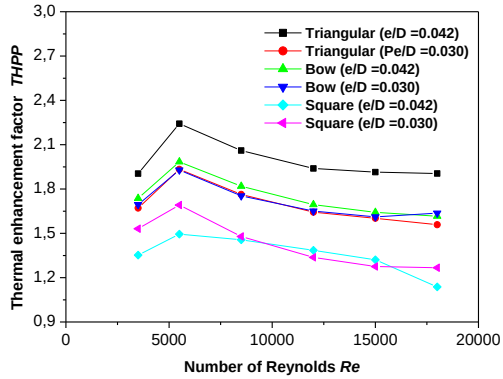

Figure 11: THPP vs. Reynolds number (*p/e* = 14.28 and *e/D* varies)

4.5. Effects of the geometric shape of the ribs

In this section, the influence of changing the shape of the ribs on enhancing the motion transfer in a thermal sensor when the fin pitch-to-height ratio is constant is compared.

It is noted that the triangular ribs significantly improve the convective heat transfer compared to the slick case and the other geometric shapes of ribs considered (see *Figure 12*). Due to its aerodynamic appearance and in the absence of acute angles, triangular ribs record the greatest energy gain (see *Figures 13* and *14*).

4.6. Distribution of the turbulent kinetic energy and turbulence intensity

The improved performance of SAHs is highly dependent on the presence of the roughness of the triangular ribs compared to the slick, square and semi-circular SAHs. The presence of artificial asperities disturbs the main flow and intensifies turbulent mixing in the inter-rib space as determined by analyzing the kinetic energy and turbulence intensity. The contours of the turbulent kinetic energy (k) and the turbulence intensity (I) are illustrated in *Figures 15* and *16*, respectively, when e/D is kept constant at 0.042, p/e = 14.28 and a wide range of Reynolds numbers ($3500 \leq Re \leq 18000$) used.

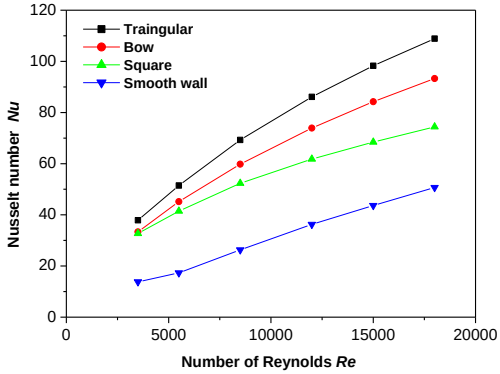

Figure 12: Relationship between the Nusselt number and Reynolds number (e/D = 0.042 and p/e = 14.28)

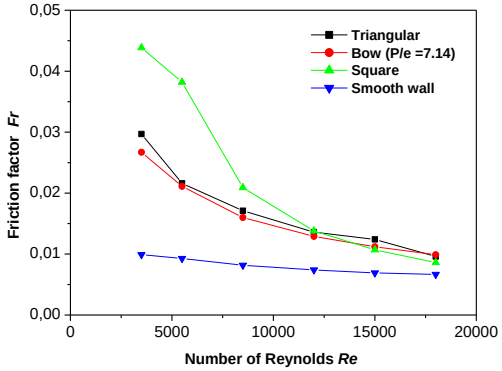

Figure 13: Friction factor vs. Reynolds number (e/D = 0.042 and p/e = 14.28)

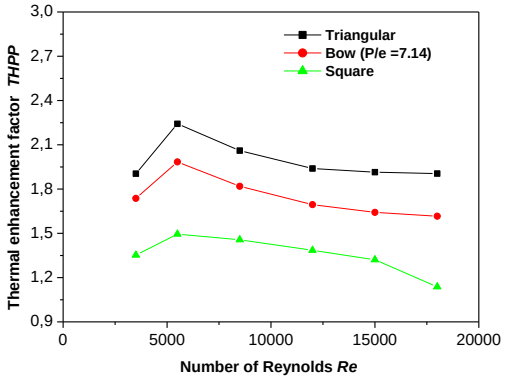

Figure 14: THPP vs. Reynolds number (p/e = 14.28 and e/D = 0.042)

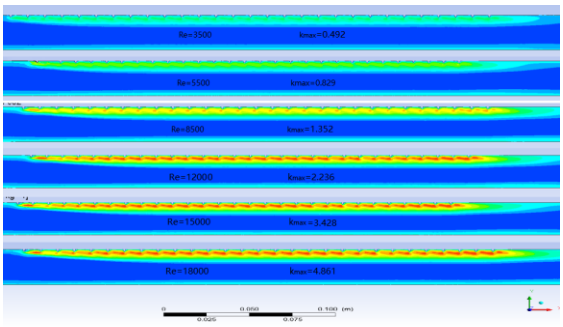

Figure 15: Visualization of the contours of the turbulent kinetic energy at different Reynolds numbers (e/D = 0.042 and p/e = 14.28)

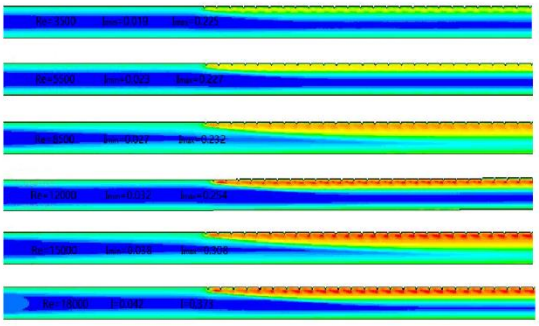

Figure 16: Visualization of the contours of the turbulence intensity when the Reynolds numbers varies (e/D = 0.042 and p/e = 14.28)

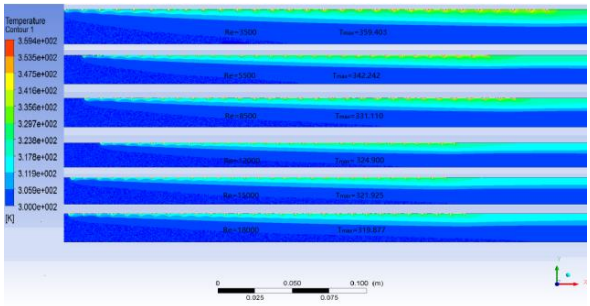

Figure 17: Static temperature contours when the Reynolds number varies (e/D = 0.042 and p/e = 14.28)

4.7. Temperature distribution

A qualitative comparison of the temperature distribution along the sensor is presented in this section. The temperature contours when the Reynolds number varies but the pitch and rib height ratios are fixed (e/D = 0.042; p/e = 14.28) is illustrated in *Figure 17*. It was observed that the gradient of the static temperature near the ribbed section de
creases as the Reynolds number increases, which can be attributed to the increased flow rate of fresh air from the inlet. This reduces the difference between the temperature of the air mass and that of the wall, thereby increasing the Nusselt number. The presence of the ribs disturbs the main flow and intensifies the convective heat transfer as the Reynolds number increases.

5. Conclusions

This numerical study investigates the thermal-hydraulic properties of a fully developed turbulent flow in a rectangular duct equipped with transverse ribs of varying geometric shapes.

In the light of this study, the subsequent conclusions can be drawn:

1. The RNG-based k-ε turbulence model adopted in this analysis yields good results and is recommended in this kind of convective heat transfer study.
2. The presence of the ribs irrespective of their geometric shape intensifies turbulent convective heat transfer and improves the thermal performance of the sensor.
3. The Nusselt number increases as the Reynolds number and relative roughness pitch increase due to the modification of the laminar sublayer of a turbulent flow in the near-wall region.
4. The maximum improvement in the Nusselt number recorded compared to the slick conduit is 53.4, 45.7 and 25.0% for the triangular, semi-circular and square ribs, respectively, when the Reynolds number was equal to 18000.
5. In all cases examined, the thermal-hydraulic performance parameter was optimal at a Reynolds number equal to 5000.
6. The improvement of the thermal-hydraulic performance parameter brought about by the presence of the triangular transverse ribs is the most important when compared to their semi-circular and square equivalents with a relative roughness pitch of 14.28 and a relative roughness height of 0.042.

Nomenclature

Nu	Nusselt number
Nu_s	Nusselt number for slick conduit
Nu_r	Nusselt number for artificially rough conduit
Re	Reynolds number
Pr	Prandtl number
e	fin thickness (mm)
D_h	hydraulic diameter of the duct (mm)
p	pitch (mm)
e/D	relative roughness height
p/e	relative roughness pitch
H	height of the duct (mm)
W	width of the duct (mm)
L	length of the duct (mm)
q	heat flux (W/m^2)
f	friction factor
f_s	friction factor for slick conduit
f_r	friction factor for artificially rough conduit
ΔP	drop in pressure (Pa)
u	air flow velocity in the x-direction (m/s)
v	air flow velocity in the y-direction (m/s)
x	distance from start of test section (m)
y	non-dimensional duct wall coordinate
T	air temperature (K)
P	pressure (Pa)
α	thermal diffusivity (m^2/s)
ρ	density of air (kg/m^3)
Q_u	heat transfer rate (W)
q_u	heat flux (W/m^2)
F_R	collector heat removal factor
A_c	gross collector area
I	incident heat flow
$(\tau\alpha)_e$	effective transmittance-absorptance product
U_L	overall heat loss coefficient
T_0	outlet temperature
T_i	inlet temperature
T_a	air temperature
T_{pm}	average wall temperature
T_{am}	average air temperature
m	flow rates
C_p	specific heat of air at constant pressure (J/kg K)
h	heat transfer coefficient
k	thermal conductivity of air (W/mK)
U	velocity of air in a duct (m/s)
$THPP$	thermal-hydraulic performance parameter/thermal enhancement factor

REFERENCES

[1] Bálint, R.; Fodor, A.; Szalkai, I.; Szalkai, Z.; Magyar, A.: Modeling and calculation of the global solar irradiance on slopes, *Hung. J. Ind. Chem.*, 2019, **47**(1), 57–63, DOI: 10.33927/hjic-2019-09

[2] Ibrahim, K.A.; Gyuk, P.M.; Aliyu, S.: The effect of solar irradiation on solar cells, *Sci. World J.*, 2019, **14**(1), 20–22

[3] Duffie, J.A.; Beckman, W.A.: Solar engineering of thermal processes (John Wiley &Sons, New York, NY, USA), 1980, ISBN: 978-0471050667

[4] Yadav, A.S.; Bhagoria, J.L.: Renewable energy sources - An application guide, *Int. J. Energy Sci.*, 2013, **3**(2), 70–90

[5] Nakhchi, M.E.; Esfahani, J.A.: Numerical investigation of rectangular-cut twisted tape insert on performance improvement of heat exchangers, *Int. J. Therm. Sci.*, 2019, **138**, 75–83, DOI: 10.1016/j.ijthermalsci.2018.12.039

[6] Sun, Z.; Zhang, K.; Li, W.; Chen, Q.; Zheng, N.: Investigations of the turbulent thermal-hydraulic performance in circular heat exchanger tubes with multiple rectangular winglet vortex generators, *Appl. Therm. Eng.,* 2020, **168**, 114838 DOI: 10.1016/j.applthermaleng.2019.114838

[7] Karima, A.; Djamel, S.; Ali, N.; Houari, A.: CFD investigations of thermal and dynamic behaviors in a tubular heat exchanger with butterfly baffles, *Front. Heat Mass Transfer,* 2018, **10**, 1–7, DOI: 10.5098/hmt.10.27

[8] Zina, B.; Filali, A.; Laouedj, S.; Benamara, N.: Numerical investigation of a solar air heater (SAH) with triangular artificial roughness having a curved top corner, *J. Appl. Fluid Mech.*, 2019, **12**(6), 1919–1928, DOI: 10.29252/JAFM.12.06.29927

[9] Han, J.C.; Zhang, Y.M.; Lee, C.P.: Augmented heat transfer in square channels with parallel, crossed and V-shaped angled ribs, *J. Heat Transfer,* 1991, **113**(3), 590–596, DOI: 10.1115/1.2910606

[10] Zhelykh, V.; Shapoval, P.; Shapoval, S.; Kasynets, M.: Influence of orientation of buildings facades on the level of solar energy supply to them, *Lect. Notes Civ. Eng. – Proc EcoComfort 2020*, 2021, **100 LNCE**, 499–504, DOI: 10.1007/978-3-030-57340-9_61

[11] Dudkiewicz, E.; Fidorów-Kaprawy, N.: The energy analysis of a hybrid hot tap water preparation system based on renewable and waste sources, *Energy*, 2017, **127**, 198–208, DOI: 10.1016/j.energy.2017.03.061

[12] Shapoval, S.; Zhelykh, V.; Spodyniuk, N.; Dzeryn, O.; Gulai, B.: The effectiveness to use the distribution manifold in the construction of the solar wall for the conditions of circulation, *Pollack Periodica*, 2019, **14**(2), 143–154, DOI: 10.1556/606.2019.14.2.13

[13] Árpád, I.: Investigation of sensible heat storage and heat insulation in the exploitation of concentrated solar energy, *Hung. J. Ind. Chem.*, 2011, **39**(2), 163–167, DOI: 10.1515/403

[14] Borbély, T.: Optimal design of high-temperature thermal energy store filled with ceramic balls, *Hung. J. Ind. Chem.*, 2012, **40**(2), 93–99, DOI: 10.1515/348

[15] Menasria, F.; Zedairia, M.; Moummi, A.: Numerical study of thermohydraulic performance of solar air heater duct equipped with novel continuous rectangular baffles with high aspect ratio, *Energy*, 2017, **133,** 593–608, DOI: 10.1016/j.energy.2017.05.002

[16] Shandal, J.; Abed, Q.A.; Al-Shamkhee, D.M.: Simulation analysis of thermal performance of the solar air/water collector by using computational fluid dynamics, *E3S Web Conf.*, 2020, **180** , 02015, DOI: 10.1051/e3sconf/202018002015

[17] Chabane; F.; Sekseff, E.: Solar air collectors with doubles glazed by different distances in support of mass flow, *Instrum. Mes. Metrol.*, 2018, **17**(1), 37–53, DOI: 10.3166/i2m.17.37-53

[18] Amraoui, M.A.; Aliane, K.: Numerical analysis of a three dimensional fluid flow in a flat plate solar collector, *Int. J. Renew. Sustain. Energy*, 2015, **3**(3), 68–75, DOI: 10.11648/j.ijrse.20140303.14

[19] Abdi, G., Amraoui, M.A.; Medjadji N.; Lorenzini, G.; Menni, Y.: 3D evaluation of a thermal and hydraulic winged solar collector, *Instrum. Mes. Metrol.*, 2022, **21**(2), 35–41, DOI: 10.18280/i2m.210201

[20] Kumar, R.; Nadda, R.; Kumar,S.; Razak, A.; Sharifpur, M.; Aybar, H. S.; Saleel, C.A.; Afzal, A.: Influence of artificial roughness parametric variation on thermal performance of solar thermal collector: An experimental study, response surface analysis and ANN modeling, *Sustain. Energy Technol. Assess.*, 2022, **52**, 102047, DOI: 10.1016/j.seta.2022.102047

[21] Daliran, A.; Ajabshirchi, Y.: Theoretical and experimental research on effect of fins attachment on operating parameters and thermal efficiency of solar air collector, *Inf. Process. Agric.*, 2018, **5**(4), 411–421, DOI: 10.1016/j.inpa.2018.07.004

[22] Promvonge, P.; Thianpong, C.: Thermal performance assessment of turbulent channel flows over different shaped ribs, *Int. Commun. Heat Mass Transfer*, 2008, **35**(10), 1327–1334, DOI: 10.1016/j.icheatmasstransfer.2008.07.016

[23] Manca, O.; Nardini, S.; Ricci, D.: Numerical analysis of water forced convection in channels with differently shaped transverse ribs, *J. Appl. Math.*, 2011, **2011**(1), 323485, DOI: 10.1155/2011/323485

[24] Manca, O.; Nardini, S.; Ricci, D.: Numerical study of air forced convection in a rectangular channel provided with ribs, *Proc. 14th Int. Heat Transfer Conf. (IHTC14),* 2010, **2**, 861–870, DOI: 10.1115/IHTC14-23244

[25] Chandra, P.R.; Alexander, C.R.; Han, J.C.: Heat transfer and friction behaviors in rectangular channels with varying number of ribbed walls, *Int. J. Heat Mass Transfer,* 2003, **46**(3), 481–495, DOI: 10.1016/S0017-9310(02)00297-1

[26] Fox, R.W.; Pritchard, P.J.; McDonald, A.T.: Introduction to Fluid Mechanics (John Wiley & Sons), 2010, ISBN: 9780470547557

[27] Kumar, A.; Saini, R.P.; Saini, J.S.: Heat and fluid flow characteristics of roughened solar air heater ducts - A review, *Renew. Energy*, 2012; **47**, 77–94, DOI: 10.1016/j.renene.2012.04.001

[28] Webb, R.L.; Eckert, E. R.G.: Application of rough surfaces to heat exchanger design, *Int. J. Heat Mass Transfer*, 1972, **15**(9), 1647–1658, DOI: 10.1016/0017-9310(72)90095-6